Ecological Indicators 107 (2019) 105551

Contents lists available at ScienceDirect

Ecological Indicators

journal homepage: www.elsevier.com/locate/ecolind

Spatial pattern of pika holes and their effects on vegetation coverage on the Tibetan Plateau: An analysis using unmanned aerial vehicle imagery

Ze Tang[a,c], Yangjian Zhang[a,b,c,*], Nan Cong[a], Michael Wimberly[d], Li Wang[e], Ke Huang[a], Junxiang Li[e], Jiaxing Zu[a,c], Yixuan Zhu[a,c], Ning Chen[a,c]

[a] Key Laboratory of Ecosystem Network Observation and Modeling, Institute of Geographic Sciences and Natural Resources Research, Chinese Academy of Sciences, Beijing 100101, China
[b] Center for Excellence in Tibetan Plateau Earth Sciences, Chinese Academy of Sciences, Beijing 100101, China
[c] College of Resources and Environment, University of Chinese Academy of Sciences, Beijing 100190, China
[d] School of Geography and Environmental Sustainability, University of Oklahoma, Oklahoma City 73019-0390, USA
[e] Peking University Shenzhen Graduate School, Shenzhen 518055, China

ARTICLE INFO

Keywords:
Pika hole
Vegetation coverage
Northern Tibet
UAV images
Object-oriented classification

ABSTRACT

The pika (*Ochotona curzoniae*) hole is an important landscape feature in the Tibetan Plateau (TP) grasslands, and it indicates grassland degradation levels due to the destruction caused by pika burrowing activities on grasslands. However, no studies have ever explored landscape patterns of pika holes and their effects on adjacent vegetation coverage. Taking meadow grasslands in Northern Tibet as an example, this study gathered unmanned aerial vehicle (UAV) images and explored landscape patterns of pika holes and their effects on grass coverage in the surroundings. The performances of two classification methods, including the decision tree classification based on Fully Constrained Least Squares (FDC) and the object-oriented classification (OBC) were compared in recognizing sizes and shapes of pika holes. The results showed that: (1) The object-oriented classification exhibits higher classification accuracy in identifying pika holes. (2) The average size of pika holes in the study area is 0.01 m^2 and they exhibit clustered distribution patterns. The average distance between any two nearest pika hole patches is 0.79 m. (3) It presents a significant quadratic relationship between the number of pika holes and grass coverage. (4) The average effective distance of pika holes on the surrounding grass coverage is 20 cm. The findings of this study can provide guidelines for pika control and improve grassland management on the TP.

1. Introduction

The Tibetan Plateau (TP), known as the "roof of the world", hosts a rich variety of unique ecosystem and is an important area for global biodiversity conservation (Huang et al., 2016; Liu et al., 2006; Sun et al., 2012). Among them, alpine meadow is the primary vegetation type and covers approximately 1.63×10^6 km^2 (Qin et al., 2015). It provides natural pasture for local stocking, and also plays a significant role for the ecological security of China in such aspects as water conservation and anti-desertification (Dong and Sherman, 2015; Yong et al., 2016).

Recently, global climate change and human activities have been causing a series of ecological consequences on the QTP (Gao et al., 2010; Huang et al., 2016; Miehe et al., 2008; Yu et al., 2012), among which grassland degradation is the most prevalent one. In parallel with grassland degradation, numerous environmental aftermaths come along, for instance, strengthened pika (*Ochotona curzoniae*) activities. Although it is generally believed that grown pika population is not the cause, but as accompanying phenomenon of meadow degradation, pikas did accelerate the grassland degradation process (Chen et al., 2017a; Smith and Foggin, 1999). One manifestation of damage caused by pika is the development of pika holes. Pika holes destroy soil structure, change soil environment, and interrupt the original pathways of material circulation and energy flow (Chen et al., 2017a; Liu et al., 2012; Yu et al., 2017). In addition, pika activities alter plant species composition, reduce plant biodiversity and biomass stock, and adversely affect the global carbon cycle (Guo et al., 2012; Zhao et al., 2013; Zhou et al., 2005). A pika can typically destroy 0.51–0.73 m^2 of

* Corresponding author at: Key Laboratory of Ecosystem Network Observation and Modeling, Institute of Geographic Sciences and Natural Resources Research, Chinese Academy of Sciences, Beijing 100101, China.
E-mail addresses: tangz.17b@igsnrr.ac.cn (Z. Tang), zhangyj@igsnrr.ac.cn (Y. Zhang), congnan@igsnrr.ac.cn (N. Cong), mcwimberly@ou.edu (M. Wimberly), wli0034@pku.edu.cn (L. Wang), huangk.13b@igsnrr.ac.cn (K. Huang), junxiang@pku.edu.cn (J. Li), zujx.15b@igsbrr.ac.cn (J. Zu), zhuyx.16s@igsnrr.ac.cn (Y. Zhu), chenn.16b@igsnrr.ac.cn (N. Chen).

https://doi.org/10.1016/j.ecolind.2019.105551
Received 14 January 2019; Received in revised form 30 June 2019; Accepted 3 July 2019
Available online 31 July 2019

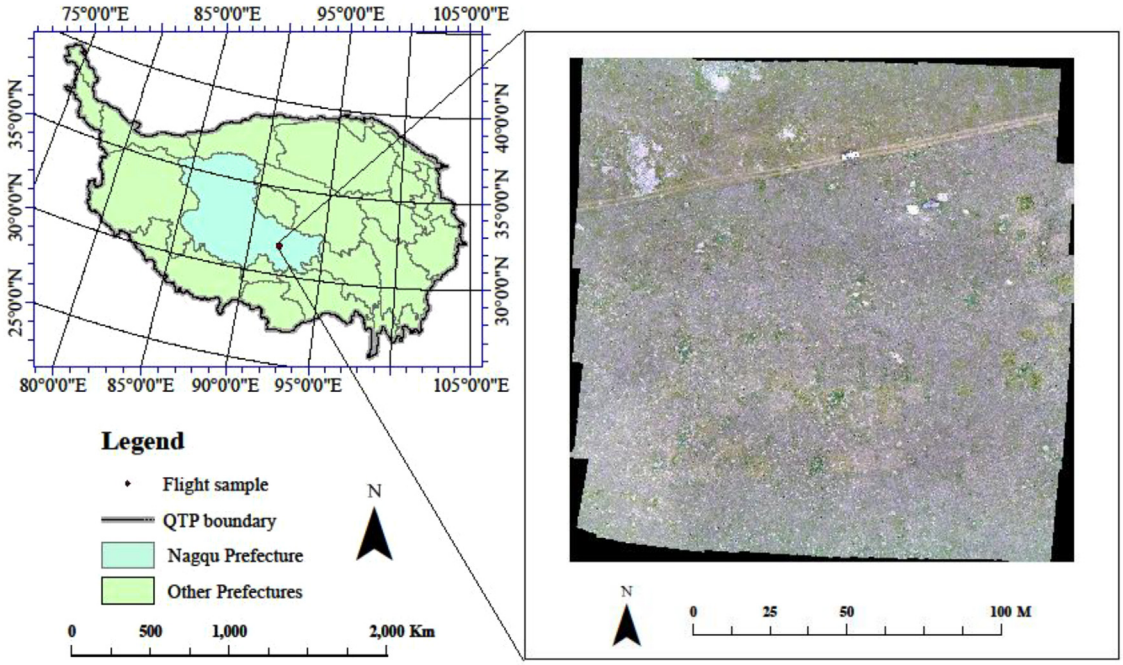

Fig. 1. Flight sample in nagqu prefecture, Tibetan Plateau (TP), China.

grassland (Chen et al., 2017a). Pikas accumulate the excavated soil outside the holes, generating environments unfavorable for grass growth. Under the strong winds and precipitation, pika holes and topsoil are eroded, aggravating the grassland degradation and fragmenting the landscape (Fig. S1). On the other hand, pika holes increase soil moisture by facilitating rainfall infiltration, and provide favorable conditions for establishment and expansion of hibernating plants (Chen et al., 2017a; Liu et al., 2012; Prejevalsky and Yule, 1991). Thus, pika holes exert varied effects on plant growth of alpine grasslands.

Traditionally, pika holes are counted using ground-based field surveys. However, this method is limited in its being laborious, lacking spatial information, and existing data gaps for harsh environments. Consequently, our understanding on relationships between pika holes and related ecological processes is highly constrained. To fully evaluate their effects, an efficient method is better developed. With the development of geospatial technologies, remote sensing has been increasingly used to study pika holes. However, prior related studies were mainly based on medium-resolution (10–80 m) data such as Landsat and CBERS images (Chen et al., 2017a; He et al., 2013; Ma et al., 2011). Their low spatial resolutions underlie their low efficiencies in identifying pika holes, thereby restricting our interpretation of their ecological consequences. Furthermore, these studies have mainly focused on the edges of the QTP, such as parts of Qinghai and Sichuan Provinces (Liu et al., 2006, 2012; Zhao et al., 2013). The Northern Tibet is one of the main distribution areas of pikas, but no studies have ever explored the landscape distribution pattern of pika holes in this region.

Remote sensing has been developed toward a stage of generating and applying high temporal and spatial resolution data (Bhardwaj et al., 2016; Van Cleemput et al., 2018; Zheng et al., 2012). As an example, unmanned aerial vehicle (UAV) remote sensing has been widely used for ecological researches (Jin et al., 2017; Puliti et al., 2017; Rey et al., 2017; Webster et al., 2018). The UAV remote sensing is a low-altitude remote sensing technology that equips unmanned aerial vehicles to carry sensors (Honkavaara et al., 2013; Qin, 2014). The vehicles are portable and suitable for various environmental conditions. The sensors mounted on the UAV can be commercial digital cameras, multispectral sensors, and radar (Bhardwaj et al., 2016; Colomina and Molina, 2014; Feng et al., 2015). Considering their loading capacity and risk control, the conventionally equipped sensors possess the characteristics of being small-sized and low cost (Du and Noguchi, 2017; Honkavaara et al., 2013; Hunt et al., 2010).

The raw images produced by digital cameras can only be used after being processed by eliminating noises and errors (Chen et al., 2017b). Then land use information can be extracted through image classification, which is primarily pixel-based. It assumes that each pixel within an image is independent, without any spatial association (Blaschke, 2001; Cleve et al., 2008; Feng et al., 2015). To solve the problem of mixed pixel, linear spectral mixture analysis has been proven efficient (Heinz et al., 1999; Liu et al., 2017; Wang et al., 2017). Among the three main algorithms of linear spectral mixture analysis, the fully constrained least squares (FCLS) algorithm is considered suitable for pixel unmixing (Chen et al., 2010; Lu and Weng, 2006; Wang et al., 2013; Weng and Lu, 2008). For fine resolution images, object-oriented classification is more efficient than the single pixel-based classification in capturing multi-pixel objects (Feng et al., 2015). The prior one divides an image into adjacent patches with homogeneity, and identifies each object according to classification rules and topological relationships (Coulter et al., 2000). The object-oriented classification also performs well in identifying landscape patterns (Cunliffe et al., 2016; Jin et al., 2017; Puliti et al., 2017).

Based on these knowledge gap and taking advantage of the recently developed remote sensing technologies, the objective of this study was to characterize the spatial distribution pattern of pika holes at a landscape scale. In the meantime, the ecological consequences of pika hole on the surrounding vegetation was explored. First, we gathered high spatial resolution remote sensing images using a UAV. Then, the performances of the above mentioned two image classification methods (the decision tree classification based on FCLS (FDC) and the object-oriented classification (OBC)) were compared in extracting pika holes information. The research findings would significantly improve our understanding on the relationships between pika activities and grass coverage on the Tibetan Plateau. The related knowledge can be used as basis for grassland management and wildlife protection on the Tibetan Plateau.

2. Study area and methods

2.1. Study area

The study area is located in Nagqu, TP (31°38.513′N, 92°0.921′E), with an approximate elevation of 4600 m (Fig. 1). The mean annual temperature is −1.2 °C and the mean annual precipitation is circa 430 mm. The air density is around 719 g/m^3, resulting in an air pressure of only 54.9 kPa. The oxygen density is roughly 166 g/m^3, equivalent to 59% of the sea level. The average annual wind speed is 37.1 m/s over the last 45 years (Luosang et al., 2017). The typical vegetation is alpine meadow, with a community height of 3–10 cm and coverage of 70–90%. The dominant species is *Kobresia pygmaea*.

2.2. Acquisition of UAV images

We flew the quadrotor Phantom 4 Pro UAV (DJI-Innovations, Shenzhen, China) at an altitude of 50 m and in a breezeless and sunny day. The flight path and image overlapping ratio are shown in Fig. S2. We obtained a total of 78 raw images. Image correction and image mosaicking were completed by the DJI-Innovations. The significant performance parameters are listed in Table S1.

2.3. Sample selection

In accordance with the purposes of this study and image quality, we used the middle part of the image and excluded those pixels tarnished by the experimental facilities and roads (Fig. 2). The entire study area is composed of two parts, with the upper part being the livestock grazing area and the lower part being the non-grazing area within the fence.

2.4. The decision tree classification based on FCLS

The FCLS algorithm of the linear spectral mixture model was first used to obtain the fraction maps of the three land categories. Firstly, the Minimum Noise Fraction (MNF) was performed prior to calculating the Pixel Purity Index (PPI). Then, an n-dimensional visualization window was built to select pure endmembers (Table S2). Finally, the unmixing process was performed.

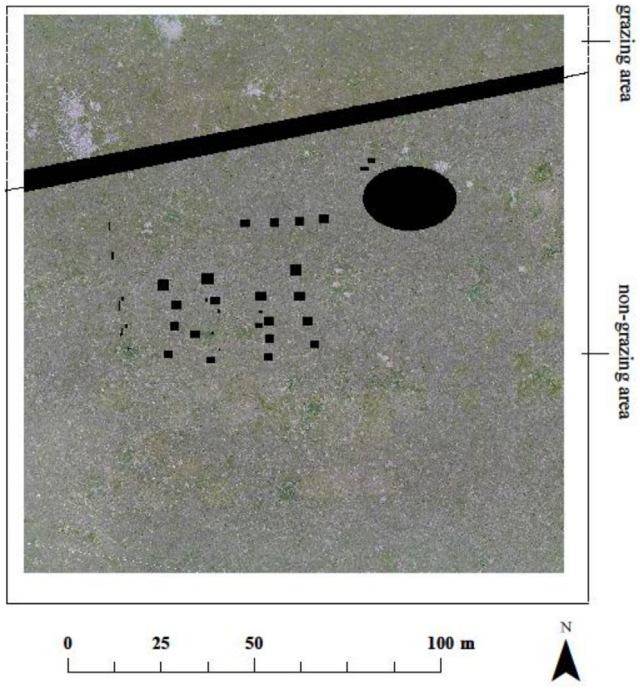

Fig. 2. Image of the study area (Black patches indicate pixels of the experimental facilities and road features).

After obtaining the fraction maps and satisfying the accuracy requirement of mean RMS < 0.02 (Fig. S3) (Tang et al., 2017), the decision tree was applied to obtain the classification map (Zhong et al., 2011). When the fraction of grass pixels exceeded 0.33, it was classified as grass; when the fraction of pika hole pixels exceeded 0.70, it was classified as pika hole. The Majority Analysis was used to eliminate small broken-up patches in the image.

2.5. Object-oriented classification

The UVA image contains only three visible bands of red, green and blue. To improve the classification accuracies, the original image was first processed by HLS transformation and principal component analysis (PCA) to construct a new image (Guo et al., 2017). The new generated data contains a total of 7 bands, including the original three color bands, three bands of HLS, and the band of the first principal component.

The object-oriented image analysis software of e-Cognition was applied in classifying the original data and the new generated data (Du and Noguchi, 2017). In both processes, all parameters were set the same. The main parameter of the scale factor was set as 15 using the Estimation of Scale Parameters (ESP) (Fig. S4) (Drăguţ et al., 2014; Drăguţ et al., 2010). The other parameters of spectrum factor, shape factor, smoothness factor and compactness factor were set as 0.9, 0.1, 0.5, 0.5, respectively (Cleve et al., 2008; Drăguţ et al., 2014).

Brightness, mean value of DN, shape index, length/width ratio and vegetation indices of excess green index (EXG), green chromatic coordinate (GCC) and visible-band difference vegetation index (VDVI) were selected as the classification features (Jin et al., 2016; Toomey et al., 2015). The nearest neighbor algorithm of standard neural networks was applied to complete the classification after calculating the best feature combination.

$$VDVI = \frac{G - R - B}{G + R + B} \quad (1)$$

$$EXG = 2 \times G - R - B \quad (2)$$

$$GCC = \frac{G}{R + G + B} \quad (3)$$

where R, G and B represent pixel values of the red band, green band, and blue band, respectively.

2.6. Accuracy assessment

The confusion matrix was used to evaluate the classification accuracy. The number of field validation points is strictly controlled, because their redundancy or inadequacy both affect the evaluation accuracy (Foody, 2009). We first determined the number of validation points according to Tortora's theory (Tortora, 1978).

$$n = B/4b^2 \quad (4)$$

where n is the number of validation points; B is the critical value of the chi-square test $(1 - \alpha/k)$ with 1-degree of freedom; α is the assessment accuracy requirement; k is the number of classifications, and b is the confidence error.

In this study, the assessment accuracy and confidence error were set at 95% and 1%, respectively. Validation points were generated randomly in ArcGIS10.5. The attribute class of each point was determined by visual interpretation to form a matrix for accuracy assessment. A total of 2550 random samples were selected, including 1026 falling in grass, 1298 in soil, and 226 in pika holes.

2.7. Landscape pattern analysis

The Fragstats 4.0 was used to explore the landscape pattern of the pika holes (McGarigal et al., 2012). The landscape indices utilized include area, number of patches (NP), patch density (PD), shape index (SHAPE), CLUMPY and COHENSION (Riitters et al., 1995). The distance between any two nearest pika hole patches was calculated and recorded as $D_{nearest}$. Then, ten concentric buffer zones with a spacing of 5 cm were generated to study the rippling effects of pika holes on adjacent landscapes. Based on their size distributions, we defined pika holes smaller than or equal to 0.01 m^2 as small type and those larger than 0.01 m^2 as large type. A 13 × 14 grid was created using the tool of fishnet in ArcGIS 10.5 to characterize landscape patterns of pika holes in each grid (Fig. S5). Regression analysis was used to fit the relationships between landscape indices of pika holes and grass coverage.

3. Result

3.1. Accuracies of the two classification methods

The new generated image contained additional color information, including hue, lightness and saturation, and some noises were also eliminated. The OBC results of the two images exhibited a high degree of similarity, but a relatively higher accuracy for the new one (Table 1). Both images produced a similar spatial pattern of grass and soil. In terms of identifying pika holes, results from the newly generated image exhibited much higher accuracies than the original image (Table 1).

The FDC result after the Majority Analysis effectively removed the 'salt and pepper' effects (Fig. 3), and the classification result was consistent with the OBC results. The FDC produced an overall accuracy of 95.57% and a kappa coefficient of 0.92, both higher than those of OBC.

3.2. Performance of each method in microscale landscape recognition

The grass area produced by the OBC was smaller than that by FDC, while the soil area was larger (Table 2). The patch number of each land-use as produced by the OBC was less than that by FDC, while the mean shape index of the prior one was greater than that of the latter (Table 2). The two methods generated distinct patterns of pika holes, although they both accurately located the position of pika holes. An entire pika hole was likely to be classified as several broken patches by the FDC. Relatively, the OBC can ensure the patch integrity and better identify microscale landscape features, such as the shape and size of pika holes.

Table 1
Accuracy assessments of the object-oriented classification (OBC) and the decision tree classification based on FCLS (FDC).

Classification method		Grass	Pika hole	Soil	User's Accuracy (%)
OBC of original image	Grass	1001	5	141	87.27
	Pika hole	7	196	56	75.97
	Soil	18	25	1101	96.24
	Producer's Accuracy (%)	97.56	86.73	84.82	
	Overall Accuracy (%)	87.17	Kappa	0.83	
OBC of newly generated image	Grass	1017	0	129	88.74
	Pika hole	0	222	7	96.94
	Soil	9	4	1162	99.06
	Producer's Accuracy (%)	99.12	98.23	89.52	
	Overall Accuracy (%)	94.16	Kappa	0.89	
FDC	Grass	1014	1	91	91.68
	Pika hole	11	216	0	95.15
	Soil	1	9	1207	99.18
	Producer's Accuracy (%)	98.83	95.58	92.99	
	Overall Accuracy (%)	95.57	Kappa	0.92	

3.3. Landscape pattern of the pika holes

The total number of pika holes for the entire study area was 4588 and covered a total area of 46 m^2 (Table 2). Pika hole sizes ranged from 0.002 m^2 to 0.074 m^2 and their average size was nearly 0.010 m^2. More than half of the pika holes covered an area between 0.002 m^2 and 0.010 m^2 (Fig. 4). The density of pika holes was 2799/ha. The shape index was 1.37, indicating their simple and regular shapes. The CLUMPY index was close to 1 and the COHESION index was close to 100, suggesting their clustered distribution and high structural connectivity among pika holes (Table 3). The distance between patch pairs ranged from 0.01 m to 4.27 m, with a mean value of 0.79 m. The $D_{nearest}$ showed their highest concentration within 0.10 m and then followed an abated frequency distribution to 1.20 m (Fig. 4).

3.4. Interaction between pika holes and vegetation coverage

There was a significant correlation between the number of pika holes and grass coverage ($P < 0.01$). When grass coverage was higher than 60%, the number of pika holes enlarged with sparser grass coverage. When the grass coverage was lower than 60%, the opposite trend was observed (Fig. 5A). Grass coverage also influenced landscape characteristics of pika holes. For each 10% increment in grass coverage, the mean size of pika holes expanded by 5 square centimeters, the CLUMPY index grew by 0.008, and the COHESNSION index rose by 0.31 (Fig. 3B–D).

Grasses exhibited a varied status in relation to the distance to pika holes. Within 20 cm, grass coverage in each buffer ring ascended with distance away from the pika hole, then eventually remained stable at around 60%. The grass coverage in each buffer ring around large pika holes was higher than that around small pika holes. Immediately adjacent to pika holes, bare soil coverage was nearly twice that of grasses (Fig. 6). Along further distance, cumulative grass coverage ascended rapidly while cumulative bare soil coverage descended. At the distance of approximately 14 cm from edges of the pika holes, grass coverage was equal to that of soil, and then surpassed it. The distance where grass coverage exceeded soil coverage was 12 cm for large pika holes and 16 cm for small pika holes. The cumulative grass coverage difference was statistically significant between areas surrounding large and small pika holes ($t = 20.286$, $df = 9$, $p < 0.001$).

4. Discussions

4.1. Efficient classification methods for high resolution images

This study compared two methods in classifying high spatial resolution images collected from UAVs. In addition, different sources of data were employed to compare the efficiencies of the OBC. Relatively, the FDC turned out higher classification accuracies than the OBC and both methods achieved high classification accuracies exceeding 94%. The traditional decision tree relies on vegetation indices for classification. However, high spatial resolution images conventionally lack infrared band to produce vegetation indices (Sandino et al., 2017; Toomey et al., 2015). The FDC method proposed in this paper first obtains the percentage of different land categories in each pixel and then determines the classification result according to their relative contribution. This algorithm can get around the limitation of totally relying on vegetation indices in classification and achieve improved accuracies. The OBC embraces information on bands of hue, lightness, saturation and the first principal component instead of texture

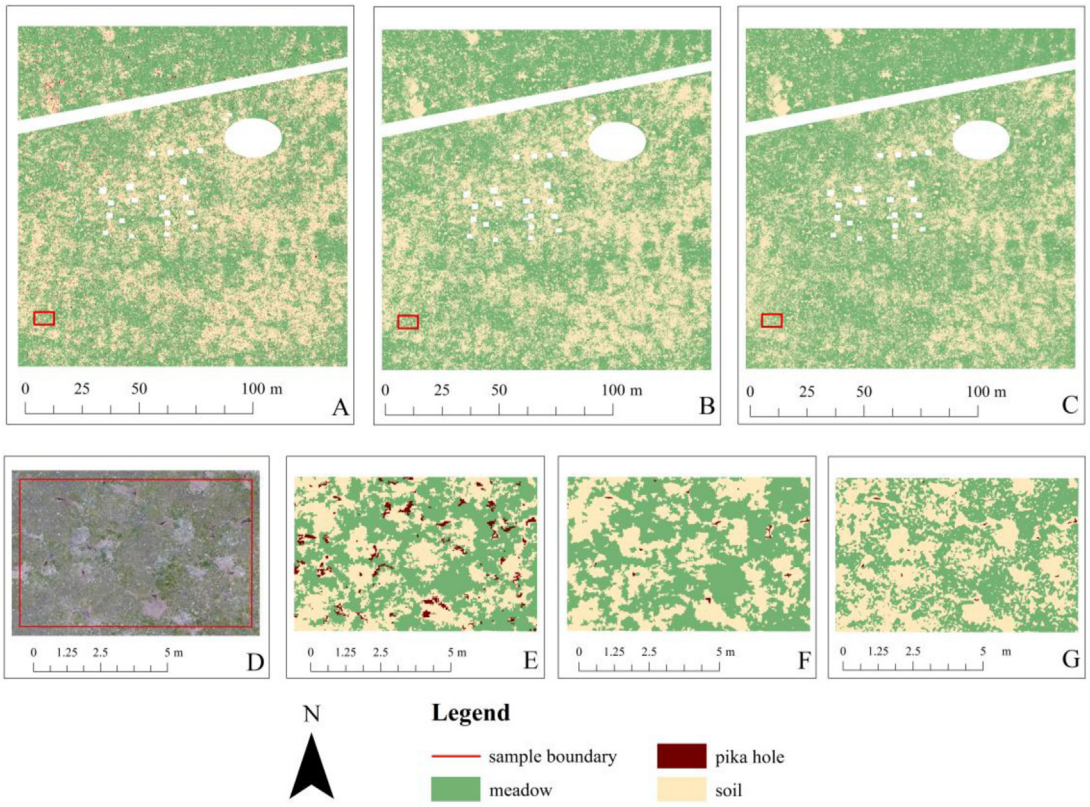

Fig. 3. The object-oriented classification (OBC) and the decision tree classification based on FCLS (FDC) results and partially enlarged details. A: OBC result of the original image, B: OBC result of the newly generated image, C: FDC result, D: image of the sample area, E: partially enlarged detail of OBC result of the original image, E: partially enlarged detail of OBC result of the newly generated image, F: partially enlarged detail of FDC result.

Table 2
The characteristics of landscape structure under different classification methods.

Source	TYPE	CA (m^2)	NP	SHAPE_MN
OBC	Grass	9118	20,294	1.91
	Soil	7346	53,638	1.53
	Pika hole	46	4588	1.37
FDC	Grass	10,246	78,991	1.26
	Soil	6228	205,154	1.25
	Pika hole	36	15,571	1.12

Note: SHAPE_MN indicates mean value of shape index.

information, and the classification accuracy was also elevated. Compared with the original image, the newly generated image can effectively reduce misclassification of wet soil and pika holes, which indicates the newly added bands can contribute extra details and widen the separability among objects. This is because the HLS transformation adjusts the expression model of colors, which is conducive to computer processing. Also, the principal component transformation serves as additional information enhancement (Dronova et al., 2015; Guo et al., 2017).

The OBC exhibited better performances in recognizing shapes and sizes of pika holes. Its segmentation algorithm ensures the shape integrity of each pika hole patch. However, the FDC likely leads to patch fragmentation. This is mainly caused by their different operating unit. The basic operation unit of the FDC is a pixel, thereby easily disregarding the integrity of ground objects and inevitably resulting in fragmentation (Cleve et al., 2008; Coulter et al., 2000; Feng et al., 2015). In addition, a fragmented patch is composed of several small broken parts and usually accompanied by simplified shapes (Heinz et al., 1999; Wang et al., 2013). That is why the FDC produced a lower

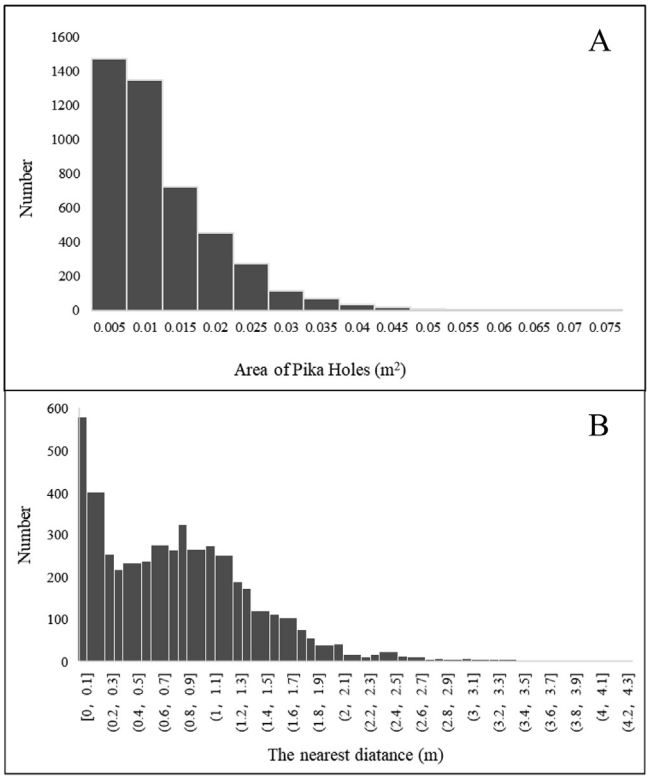

Fig. 4. Frequency distribution of pika hole sizes (A) and $D_{nearest}$ (B).

Table 3
Landscape characteristics of the pika hole.

PD (n/ha)	Area_MN (m^2)	CLUMPY	COHENSION
2779	0.01	0.81	87.67

Note: Area_MN indicates mean area of pika hole patches.

shape index. Collectively, the OBC is more suitable for identifying shape and size of pika holes on the Tibetan Plateau.

4.2. Spatial pattern of the pika hole

For the meadow targeted in this study, the pika hole density is 2779/ha. This value is higher than those reported for fringe zones of the Tibetan Plateau. The density of pika holes in Qinghai Province is circa 500–3600/ha, of which most studies reported a value of 1000–1600/ha (Guo et al., 2012; Li and Zhang, 2006; Liu et al., 2014; Zhao et al., 2013). The pika hole has an average size of approximately 0.01 m^2 and their shapes are relatively simpler compared to those of grasses and bare soil. The mean size value is in line with results obtained from field surveys in other regions of the QTP (Ma et al., 2011; Pech et al., 2007b; Wang et al., 1998).

This study further explored the landscape pattern of pika holes. A value of the CLUMPY index closer to 1 represents the higher aggregation of the patch distribution. The CLUMPY index value of 0.81 in this study indicated the clustered distribution of pika holes. Such a spatial pattern is related to the limited resources available to pikas. They mainly feed on grasses, sedges and legumes and prefer to live in environments with wide horizons (Chen et al., 2017a; Harris, 2010; Marcfoggin, 2010). The inhomogeneous living conditions lead to their tendencies of clumped presences. The landscape analysis also revealed the high structural connectivity of pika holes, which facilitates pika movements in escaping predators.

4.3. Influences of pika activities on meadow coverage

For the first time, this paper reported the effects of vegetation coverage on pika holes at a landscape scale, and vice versa. The number of pika holes varied unimodally with vegetation coverage. When grass coverage increases or decreases from a certain threshold, the number of pika holes abates. This interaction reveals that pika presence is more likely to be affected by grass coverage, rather than the other way around (Harris, 2010). Only when grassland degrades to a certain extent, the number of pika holes erupts. Mean area of pika hole patches, CLUMPY index and COHENSION index all increase with elevated grass coverage. This pattern may be explained by the resource carrying capacity. The enriched biomass caused by elevated grass coverage can feed larger populations of pikas, which burrow an increased number of pika holes, thereby causing their more clumped pattern (Badingquiying et al., 2018; Liu et al., 2009).

The nonlinear relationship between the number of pika holes with vegetation coverage is related to the living habits of pikas. They tend to live in areas with lower grass height and open fields (Badingquiying et al., 2018; Liu et al., 2013). Dense grasslands would undermine their capability of escaping and boost the danger of being preyed (Liu, 2003). Only when grasslands are degraded by other factors such as grazing and human disturbance, can a wider horizon of vision be formed. The growing population of pikas further exacerbates grassland degradation (Harris et al., 2015), which downgrades food resources availability, eventually declined pika populations.

Previous studies have proved that sole rodent control has low efficiency in alleviating grassland degradation. The pika population can still recover after ceasing of rodent control (Pech et al., 2007a). Increasing vegetation coverage may be a more feasible and ecological pathway in practice management to control the pika population (Fig. 5). By acting on environments, pika holes indirectly affect vegetation growth in the surroundings (Smith and Foggin, 1999; Zhao et al., 2013). In the vicinity of pika holes, bare soil covered area is much larger than by grasses. This pattern might be caused by two major reasons. First, pika graze on and trample meadows (Chen et al., 2017a; Zhao et al., 2013). Second, pika holes modify physical and chemical properties of soils, consequently affecting grasses growth (Li and Zhang, 2006; Liu et al., 2012; Yu et al., 2017). Therefore, in areas closer to pika holes, the lower is grass coverage. Along further away distance, environmental influences of pika holes fades, and grass coverage rises. When the distance exceeds 20 cm away, their influences basically disappear and grass coverage re-bounces to a normal level.

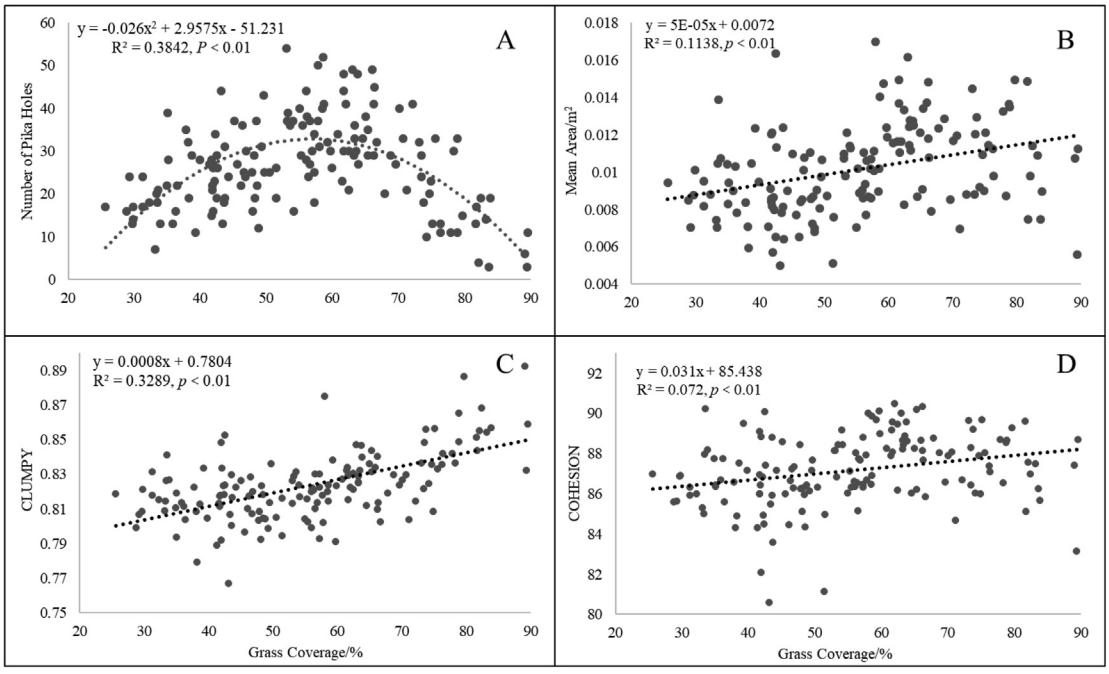

Fig. 5. Relationship between grass coverage and number of pika holes (A), mean area of pika holes (B), CLUMPY index (C) and COHENSION index (D).

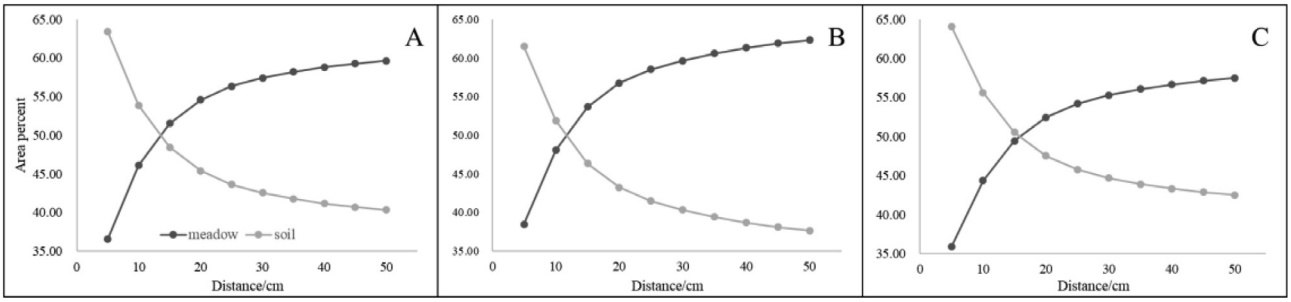

Fig. 6. The cumulative percentage of grass area and soil area with distance away from pika holes. A: all pika holes, B: pika holes with area larger than 0.01 m^2 (large pika holes), C: pika holes with area less than or equal to 0.01 m^2 (small pika holes).

Different from conventional viewpoints, this study showed that small pika holes exert greater influences on grass coverage in the surroundings than large pika holes do. The reason is related to the existence duration of pika holes. Most of small pika holes are formed in the current year and the effects of excavation behavior on the surrounding vegetation still persist. While most of large pika holes are developed from the initial small ones and have been already existed for some periods. Vegetation around the large pika hole has been recovered to some extents due to the gradually abated pika disturbance and succession of ecosystem (Komonen et al., 2003). Therefore, grass coverage around large pika holes can be higher than that around small pika holes.

5. Conclusion

For the first time this study investigated the landscape pattern of pika holes and their effects on surrounding vegetation growth on the Tibetan Plateau by utilizing high resolution data of UAVs. The pattern of pika holes is an important factor affecting grasslands in northern Tibet, and it is bound to be of great significance for understanding the changes of the ecosystem. The following findings can be theory basis for pika control and ecosystem management on the Tibetan Plateau. First, the decision tree classification based on FCLS achieves the highest classification accuracy of 95.57%. The object-oriented classification performs best in identifying the shape and size of objects. Second, pika hole density on the targeted meadow is higher than other parts of the Tibetan Plateau. Third, pika hole presence is more likely to be consequences of grassland degradation, rather than causing grassland degradation.

Funding

This work was supported by Optimized Allocation System and Model of Grassland Ecology and Production in Tibetan Plateau [grant number 2016YFC0502001]; the International Partnership Program of Chinese Academy of Sciences [grant number 131C11KYSB20160061]; and National Natural Science Foundation of China [grant number 41725003].

Declaration of Competing Interest

None.

Appendix A. Supplementary data

Supplementary data to this article can be found online at https://doi.org/10.1016/j.ecolind.2019.105551.

References

Badingquiying, Smith, A.T., Harris, R.B., 2018. Summer habitat use of plateau pikas (Ochotona curzoniae) in response to winter livestock grazing in the alpine steppe Qinghai-Tibetan Plateau. Arctic Antarct. Alpine Res. 50, e1447190.

Bhardwaj, A., Sam, L., Akanksha, Martín-Torres, F.J., Kumar, R., 2016. UAVs as remote sensing platform in glaciology: present applications and future prospects. Remote Sens. Environ. 175, 196–204.

Blaschke, T., 2001. What's wrong with pixels? Some recent developments interfacing remote sensing and GIS. GeoBIT/GIS 6, 12–17.

Chen, F., Qiu, Q., Xiong, Y., Huang, S., 2010. Pixel unmixing based on linear spectral mixture model: methods and comparison. Remote Sens. Inform. 4, 22–28.

Chen, J., Yi, S., Qin, Y., 2017a. The contribution of plateau pika disturbance and erosion on patchy alpine grassland soil on the Qinghai-Tibetan Plateau: implications for grassland restoration. Geoderma 297, 1–9.

Chen, S., McDermid, G., Castilla, G., Linke, J., 2017b. Measuring vegetation height in linear disturbances in the boreal forest with UAV photogrammetry. Remote Sens. 9, 1257.

Cleve, C., Kelly, M., Kearns, F.R., Moritz, M., 2008. Classification of the wildland-urban interface: a comparison of pixel- and object-based classifications using high-resolution aerial photography. Comput. Environ. Urban Syst. 32, 317–326.

Colomina, I., Molina, P., 2014. Unmanned aerial systems for photogrammetry and remote sensing: a review. ISPRS J. Photogramm. Remote Sens. 92, 79–97.

Coulter, L., Stow, D., Hope, A., O'Leary, J., Turner, D., Longmire, P., Peterson, S., Kaiser, J., 2000. Comparison of high spatial resolution imagery for efficient generation of GIS vegetation layers. Photogramm. Eng. Remote Sens. 66, 1329–1336.

Cunliffe, A.M., Brazier, R.E., Anderson, K., 2016. Ultra-fine grain landscape-scale quantification of dryland vegetation structure with drone-acquired structure-from-motion photogrammetry. Remote Sens. Environ. 183, 129–143.

Dong, S., Sherman, R., 2015. Enhancing the Resilience of COUPLED Human and NATURAL Systems of ALPINE Rangelands on the Qinghai-Tibetan Plateau. CSIRO.

Drăguţ, L., Csillik, O., Eisank, C., Tiede, D., 2014. Automated parameterisation for multi-scale image segmentation on multiple layers. Isprs J Photogramm Remote Sens 88, 119–127.

Drăguţ, L., Tiede, D., Levick, S.R., 2010. ESP: a tool to estimate scale parameter for multiresolution image segmentation of remotely sensed data. Int. J. Geograph. Inform. Sci. 24, 859–871.

Dronova, I., Gong, P., Wang, L., Zhong, L., 2015. Mapping dynamic cover types in a large seasonally flooded wetland using extended principal component analysis and object-based classification. Remote Sens. Environ. 158, 193–206.

Du, M., Noguchi, N., 2017. Monitoring of wheat growth status and mapping of wheat yield's within-field spatial variations using color images acquired from UAV-camera system. Remote Sens. 9, 289.

Feng, Q., Liu, J., Gong, J., 2015. UAV remote sensing for urban vegetation mapping using random forest and texture analysis. Remote Sens. 7, 1074–1094.

Foody, G.M., 2009. Sample size determination for image classification accuracy assessment and comparison. Int. J. Remote Sens. 30, 5273–5291.

Gao, Q.-Z., Wan, Y.-F., Xu, H.-M., Li, Y., Jiangcun, W.-Z., Borjigidai, A., 2010. Alpine grassland degradation index and its response to recent climate variability in Northern Tibet, China. Quat. Int. 226, 143–150.

Guo, P., Wu, F., Dai, J., Wang, H., Xu, L., Zhang, G., 2017. Comparison of farmland crop classification methods based on visible light images of unmanned aerial vehicles. Trans. Chin. Soc. Agric. Eng. 33, 112–119.

Guo, Z.G., Li, X.F., Liu, X.Y., Zhou, X.R., 2012. Response of alpine meadow communities to burrow density changes of plateau pika (Ochotona curzoniae) in the Qinghai-Tibet Plateau. Acta Ecol. Sin. 32, 44–49.

Harris, R.B., 2010. Rangeland degradation on the Qinghai-Tibetan plateau: a review of the evidence of its magnitude and causes. J. Arid Environ. 74, 1–12.

Harris, R.B., Wenying, W., Badinqiuying, SmithA.T., Bedunah, D.J., 2015. Herbivory and competition of tibetan steppe vegetation in winter pasture: effects of livestock exclosure and plateau pika reduction. PLoS One 10, e0132897.

He, Y., Huang, X., Hou, X., Feng, Q., Wang, W., Guo, Z., Liang, T., 2013. Monitoring grassland rodents with 3S technologies. Acta Pratacult. Sin. 22, 33–40.

Heinz, D., Chang, C.-I., Althouse, M.L., 1999. Fully constrained least-squares based linear unmixing [hyperspectral image classification], Geoscience and Remote Sensing Symposium, 1999. IGARSS'99 Proceedings. IEEE 1999 International. IEEE, pp. 1401–1403.

Honkavaara, E., Saari, H., Kaivosoja, J., Pölönen, I., Hakala, T., Litkey, P., Mäkynen, J., Pesonen, L., 2013. Processing and assessment of spectrometric, stereoscopic imagery collected using a lightweight UAV spectral camera for precision agriculture. Remote

Sens. 5, 5006–5039.
Huang, K., Zhang, Y., Zhu, J., Liu, Y., Zu, J., Zhang, J., 2016. The influences of climate change and human activities on vegetation dynamics in the qinghai-tibet plateau. Remote Sens. 8, 876.
Hunt, E.R., Hively, W.D., Fujikawa, S., Linden, D., Daughtry, C.S., McCarty, G., 2010. Acquisition of NIR-green-blue digital photographs from unmanned aircraft for crop monitoring. Remote Sens. 2, 290–305.
Jin, R., Deng, L., Zhao, W., Gong, Z., 2016. Object-oriented aquatic vegetation extracting approach based on visible vegetation indices. Chin. J. Appl. Ecol. 27, 1427–1436.
Jin, X., Liu, S., Baret, F., Hemerlé, M., Comar, A., 2017. Estimates of plant density of wheat crops at emergence from very low altitude UAV imagery. Remote Sens. Environ. 198, 105–114.
Komonen, Minna, Komonen, Atte, Otgonsuren, Avirmed, 2003. Daurian pikas (Ochotona daurica) and grassland condition in eastern Mongolia. J. Zool. 259, 281–288.
Li, W., Zhang, Y., 2006. Impacts of plateau pikas on soil organic matter and moisture content in alpine meadow. Acta Theriol. Sin. 26, 331–337.
Liu, H., Chen, Y., Li, Z., Zhen, J., Mcm, J., Pika, P., Control, L., 2013. The effects of management on population dynamics of plateau pika. Math. Comput. Modell. 57, 525–535.
Liu, J., Wu, Z., Xiao, Z., Yang, J., 2017. Classification of hyperspectral images using kernel fully constrained least squares. ISPRS Int. J. Geo-Inf. 6, 344.
Liu, L., Zhang, Y., Bai, W., Yan, J., Ding, M., Shen, Z., Li, S., Zheng, D., 2006. Characteristics of grassland degradation and driving forces in the source region of the Yellow River from 1985 to 2000. J. Geog. Sci. 16, 131–142.
Liu, W., 2003. Studies on destruction, prevention and control of plateau pikas in kobresia pygmaea meadow. Acta Theriol. Sin. 23, 214–219.
Liu, W., Yan, Z., Wang, X., Wang, C., 2014. Effects of plateau pikas on restoring succession of degraded grassland and plant community structure. Acta Theriol. Sin. 34, 54–61.
Liu, W., Zhang, Y., Wang, X., Zhao, J., Qingmin, X.U., Zhou, L., 2009. The relationship of the harvesting behavior of plateau pikas with the plant community. Acta Theriol. Sin. 29, 40–49.
Liu, Y., Fan, J., Harris, W., Shao, Q., Zhou, Y., Wang, N., Li, Y., 2012. Effects of plateau pika (Ochotona curzoniae) on net ecosystem carbon exchange of grassland in the Three Rivers Headwaters region, Qinghai-Tibet, China. Plant Soil 366, 491–504.
Lu, D., Weng, Q., 2006. Use of impervious surface in urban land-use classification. Remote Sens. Environ. 102, 146–160.
Luosang, Z., Badan, Z., Pubu, Z., Bianma, L., Yongzhu, Z., 2017. Analysis of climate change and basic meteorological elements in nagqu prefecture in recent 45 Years. Tibet's Sci. Technol. 10, 60–62.
Ma, B., Wang, X., Liu, X., Wang, Z., 2011. GIS analysis of the spatial relationship between plateau pika burrow distribution and vegetation distributional patterns. Biodivers. Sci. 19.
Marcfoggin, J., 2010. The plateau pika (Ochotona curzoniae) is a keystone species for biodiversity on the Tibetan plateau. Anim. Conserv. 2, 235–240.
McGarigal, K., Cushman, S.A., Ene, E., 2012. FRAGSTATS v4: spatial pattern analysis program for categorical and continuous maps. Computer software program produced by the authors at the University of Massachusetts, Amherst. Available at: http://www. umass.edu/landeco/research/fragstats/fragstats.html.
Miehe, G., Miehe, S., Kaiser, K., Jianquan, L., Zhao, X., 2008. Status and dynamics of the kobresia pygmaea ecosystem on the tibetan plateau. AMBIO J. Hum. Environ. 37, 272–279.
Pech, R., Jiebu, Arthur, A., Zhang, Y., Hui, L., 2007a. Population dynamics and responses to management of plateau pikas Ochotona curzoniae. J. Appl. Ecol. 44, 615–624.
Pech, R.P., Arthur, A.D., Yanming, Z., Hui, L., 2007b. Population dynamics and responses to management of plateau pikas Ochotona curzoniae. J. Appl. Ecol. 44, 615–624.
Prejevalsky, N., Yule, H., 1991. Mongolia: The Tangut Country and the Solitudes of Northern Tibet. Asian Educational Services.
Puliti, S., Ene, L.T., Gobakken, T., Næsset, E., 2017. Use of partial-coverage UAV data in sampling for large scale forest inventories. Remote Sens. Environ. 194, 115–126.
Qin, R., 2014. An object-based hierarchical method for change detection using unmanned aerial vehicle images. Remote Sens. 6, 7911–7932.
Qin, Y., Yi, S., Chen, J., Ren, S., Ding, Y., 2015. Effects of gravel on soil and vegetation properties of alpine grassland on the Qinghai-Tibetan plateau. Ecol. Eng. 74, 351–355.
Rey, N., Volpi, M., Joost, S., Tuia, D., 2017. Detecting animals in African savanna with UAVs and the crowds. Remote Sens. Environ. 200, 341–351.
Riitters, K.H., O'neill, R., Hunsaker, C., Wickham, J.D., Yankee, D., Timmins, S., Jones, K., Jackson, B., 1995. A factor analysis of landscape pattern and structure metrics. Landsc. Ecol. 10, 23–39.
Sandino, J., Wooler, A., Gonzalez, F., 2017. Towards the AUTOMATIC DETECTION OF PRE-EXISTING TERMITE MOUNDS THROUGH UAS AND HYPERSPECTRAL IMAGEry. Sensors (Basel) 17.
Smith, A.T., Foggin, J.M., 1999. The plateau pika (Ochotona curzoniae) is a keystone species for biodiversity on the Tibetan plateau. Anim. Conserv. 2, 235–240.
Sun, H., Zheng, D., Yao, T., Zhang, Y., 2012. Protection and construction of the national ecological security shelter zone on tibetan plateau. Acta Geographica Sinica 67, 3–12.
Tang, Z., Zheng, H., Ren, Z., Zhang, D., Wang, P., Zhai, C., Cui, M., He, X., 2017. Evaluating environmental equities of urban forest in terms of cooling services using ETM+ and Google data. J. Indian Soc. Remote Sens. 1–10.
Toomey, M., Friedl, M.A., Frolking, S., Hufkens, K., Klosterman, S., Sonnentag, O., Baldocchi, D.D., Bernacchi, C.J., Biraud, S.C., Bohrer, G., 2015. Greenness indices from digital cameras predict the timing and seasonal dynamics of canopy-scale photosynthesis. Ecol. Appl. A Publ. Ecol. Soc. Am. 25, 99.
Tortora, R., 1978. A note on sample size estimation for multinomial populations. Am. Stat. 32, 100–102.
Van Cleemput, E., Vanierschot, L., Fernández-Castilla, B., Honnay, O., Somers, B., 2018. The functional characterization of grass- and shrubland ecosystems using hyperspectral remote sensing: trends, accuracy and moderating variables. Remote Sens. Environ. 209, 747–763.
Wang, L., Liu, D., Wang, Q., 2013. Geometric method of fully constrained least squares linear spectral mixture analysis. IEEE Trans. Geosci. Remote Sens. 51, 3558–3566.
Wang, M., Zhong, W., Wan, X., Wang, G., 1998. Habitat selection during dispersion of Daurian pika (Ochotona daurica). Acta Zool. Sin.
Wang, X., Zhong, Y., Zhang, L., Xu, Y., 2017. Spatial group sparsity regularized nonnegative matrix factorization for hyperspectral unmixing. IEEE Trans. Geosci. Remote Sens. 55, 6287–6304.
Webster, C., Westoby, M., Rutter, N., Jonas, T., 2018. Three-dimensional thermal characterization of forest canopies using UAV photogrammetry. Remote Sens. Environ. 209, 835–847.
Weng, Q., Lu, D., 2008. A sub-pixel analysis of urbanization effect on land surface temperature and its interplay with impervious surface and vegetation coverage in Indianapolis, United States. Int. J. Appl. Earth Observ. Geoinform. 10, 68–83.
Yong, Z., Dong, S., Gao, Q., Liu, S., Yan, L., Cao, X., 2016. Responses of alpine vegetation and soils to the disturbance of plateau pika (Ochotona curzoniae) at burrow level on the Qinghai-Tibetan Plateau of China. Ecol. Eng. 88, 232–236.
Yu, C., Zhang, J., Pang, X.P., Wang, Q., Zhou, Y.P., Guo, Z.G., 2017. Soil disturbance and disturbance intensity: response of soil nutrient concentrations of alpine meadow to plateau pika bioturbation in the Qinghai-Tibetan Plateau, China. Geoderma 307, 98–106.
Yu, C., Zhang, Y., Claus, H., Zeng, R., Zhang, X., Wang, J., 2012. Ecological and environmental issues faced by a developing Tibet. Environ. Sci. Technol. 46, 1979–1980.
Zhao, G., Li, G., Ma, W., Zhao, D., Li, X., 2013. Impacts of Ochotona pallasi disturbance on alpine grassland community characteristics. Chin. J. Appl. Ecol. 24, 2122–2128.
Zheng, B., Campbell, J.B., de Beurs, K.M., 2012. Remote sensing of crop residue cover using multi-temporal Landsat imagery. Remote Sens. Environ. 117, 177–183.
Zhong, L., Hawkins, T., Biging, G., Gong, P., 2011. A phenology-based approach to map crop types in the San Joaquin Valley, California. Int. J. Remote Sens. 32, 7777–7804.
Zhou, H., Zhao, X., Zhou, L., Liu, W., Li, Y., Tang, Y., 2005. A study on correlations between vegetation degradation and soil degradation in the Alpine Meadow of the Qinghai-Tibetan Plateau. Acta Pratacult. Sin. 14, 31–40.